JACS
JOURNAL OF THE AMERICAN CHEMICAL SOCIETY
Article
pubs.acs.org/JACS

# Experimental Quantification of Electrostatics in X−H···π Hydrogen Bonds

Miguel Saggu,* Nicholas M. Levinson,* and Steven G. Boxer*

Department of Chemistry, Stanford University, Stanford, California 94305-5012, United States

Supporting Information

**ABSTRACT:** Hydrogen bonds are ubiquitous in chemistry and biology. The physical forces that govern hydrogen-bonding interactions have been heavily debated, with much of the discussion focused on the relative contributions of electrostatic vs quantum mechanical effects. In principle, the vibrational Stark effect, the response of a vibrational mode to electric field, can provide an experimental method for parsing such interactions into their electrostatic and nonelectrostatic components. In a previous study we showed that, in the case of relatively weak O−H···π hydrogen bonds, the O−H bond displays a linear response to an electric field, and we exploited this response to demonstrate that the interactions are dominated by electrostatics (Saggu, M.; Levinson, N. M.; Boxer, S. G. *J. Am. Chem. Soc.* **2011**, *133*, 17414−17419). Here we extend this work to other X−H···π interactions. We find that the response of the X−H vibrational probe to electric field appears to become increasingly nonlinear in the order O−H < N−H < S−H. The observed effects are consistent with differences in atomic polarizabilities of the X−H groups. Nonetheless, we find that the X−H stretching vibrations of the model compounds indole and thiophenol report quantitatively on the electric fields they experience when complexed with aromatic hydrogen-bond acceptors. These measurements can be used to estimate the electrostatic binding energies of the interactions, which are found to agree closely with the results of energy calculations. Taken together, these results highlight that with careful calibration vibrational probes can provide direct measurements of the electrostatic components of hydrogen bonds.

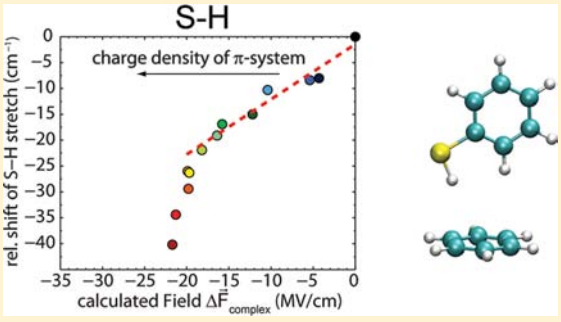


## INTRODUCTION

Hydrogen bonds are ubiquitous in all aspects of chemistry, biology, and materials science.[1−3] Conventional hydrogen bonds are defined as X−H···A, where the acceptor A and the donor X are usually very electronegative (O, N, and F are most frequently encountered). A well-established classification groups hydrogen bonds into three categories: weak, moderate, and strong hydrogen bonds with dissociation energies varying between 0.5−40 kcal/mol.[1] The total dissociation energy can be considered to arise from different effects including electrostatics, polarization, charge transfer, dispersion, and exchange repulsion (the latter two are often combined to the isotropic van der Waals interaction),[4,5] whose relative contributions vary widely among hydrogen bonds and depend on the particular donor−acceptor characteristics.[5] The electrostatic term describes the interaction between all permanent charges and multipoles, such as dipole−dipole or dipole−quadrupole, and the polarization term describes the interactions between all permanent charges and induced multipoles, such as dipole−induced dipole, while the dispersion term describes all interactions between induced multipoles, such as induced dipole−induced dipole. While all of the individual contributions have different distance dependencies, the electrostatic part decays slowest with distance ($r^{-3}$ for a dipole−dipole interaction) and becomes more important in longer and weaker hydrogen bonds.

The moderate class of hydrogen bonds, generally formed between an electronegative donor X and acceptor A, e.g., N−H···O or N−H···N, is the predominant form of hydrogen bonds in biological molecules. This class of interactions is responsible for the structure of water and ice, the formation of protein secondary structures, and nucleic acid base pairing. The bond energies of this class of hydrogen bonds vary between 4 and 15 kcal/mol.[1,3,5] Although a lot of attention is focused on these moderate hydrogen bonds, another type of hydrogen bond, in which π-systems play the role of the acceptor, is important in biological systems. These interactions belong to the weak class of hydrogen bonds, with dissociation energies <4 kcal/mol[1,2,6] and include C−H···π interactions, which are widespread in crystal packing and are found in the hydrophobic cores of protein structures, where they stabilize the interactions between aromatic residues.[2,7,8] Statistical analysis of the protein databank has shown that O−H···π, N−H···π, C−H···π, and S−H···π interactions all occur frequently in proteins.[6,8,9] From theoretical studies it has been proposed that the electrostatic contribution to π-hydrogen bonding for different hydrogen-bond donors decreases in the order of O−H ≈ S−H > N−H > C−H due to the differences in partial charges,[10,11] while the dispersion contribution decreases in the order of S−H > C−H

**Received:** June 8, 2012
**Published:** October 25, 2012

   dx.doi.org/10.1021/ja305575t | J. Am. Chem. Soc. 2012, 134, 18986−18997

> N−H > O−H due to trends in atomic polarizabilites (sulfur has a three times larger polarizability than oxygen and nitrogen).[10−14]

While the dissociation enthalpies $\Delta H^0$ or free energies $\Delta G^0$ of $\pi$-hydrogen bonds are reported in the literature for some cases, e.g., phenol with different benzene derivatives, what is missing to date is an experimental approach that can quantify the individual energetic contributions to binding.[15,16] In principle, vibrational Stark spectroscopy, which permits experimental measurements of electric fields, can be used to quantify the electrostatic contribution to hydrogen bonding, thereby parsing these interactions into their electrostatic and nonelectrostatic components. Electric fields of any origin, e.g., arising from the solvent or externally applied, perturb molecular vibrations, and the observed peak shifts can be converted into changes of electric fields if the sensitivity of the vibrational probe to field has been calibrated by vibrational Stark spectroscopy, as shown in numerous previous studies on nitriles, carbonyls, and other probes in proteins and model systems.[17−19]

In a previous study we quantified the electrostatic component of O−H···$\pi$ interactions between phenol and a series of benzene-based aromatic solvents, using a combination of vibrational Stark spectroscopy and density functional theory (DFT) calculations.[16] The response of the O−H stretch to electric field was found to be linear within the range of fields investigated, and we showed that the O−H···$\pi$ interactions are dominated by electrostatics, as opposed to other effects. Here we extend this work to N−H···$\pi$ and S−H···$\pi$ interactions. We used indole (N−H) and thiophenol (S−H) as hydrogen-bond donors, where the linear X−H groups serve as vibrational probes to report on electric fields experienced upon formation of hydrogen bonds with aromatic systems (see Figure 1) and where the sensitivity of the X−H vibration to electric fields can be calibrated by vibrational Stark spectroscopy.[17]

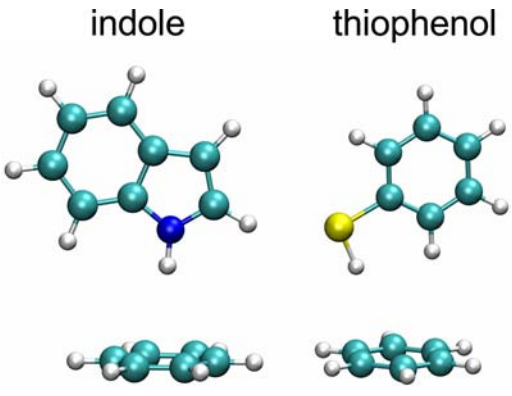


**Figure 1.** Structures of the different X−H···$\pi$ complexes investigated in this study.

We show that both probes measure the electrostatic component of X−H···$\pi$ interactions, allowing an experimental separation of the electrostatic term from the nonelectrostatic components. The results show that the strength of the electrostatic interactions decreases in the order O−H > N−H > S−H and can be as large as ∼3 kcal/mol for the strongest complexes.

The sensitivity of vibrational groups to electric field, quantified by the linear Stark tuning rate $\Delta\vec{\mu}$, is generally assumed to be roughly constant, i.e., an intrinsic property of the oscillator with little if any dependence on specific chemical interactions, as shown in extensive studies on nitriles.[17,20] We show here that in the case of highly polarizable groups like S−H, the assumption of a constant linear Stark tuning rate is not valid, and its magnitude is field dependent in the strongest complexes. Variations in the linear Stark tuning rate of up to 40% are observed for the S−H stretch in S−H···$\pi$ interactions, depending on the strength of the interaction. In the case of the moderate hydrogen-bond regime, represented here by X−H···O and X−H···N interactions, dramatic increases in the sensitivity of both N−H and S−H vibrational probes are observed (up to 3-fold), highlighting the need for careful calibration of vibrational probes when used to study stronger chemical interactions.

## MATERIALS AND METHODS

**Chemicals.** All chemicals were purchased from Sigma-Aldrich (St. Louis, MO) and of highest available purity. Indole, pyrrole, and thiophenol were dissolved in different benzene derivatives to form X−H···$\pi$ complexes with final concentrations of 20 mM for indole and pyrrole and 200 mM for thiophenol. The strength of the complexes was controlled by changing the charge density of the benzene $\pi$-system acceptors using electron-withdrawing chlorine or electron-donating methyl groups. Most of these benzene derivatives were liquid except for 1,2,4,5-tetramethylbenzene, pentamethylbenzene, and hexamethylbenzene. In order to compare all complexes under identical conditions, the hydrogen donors were dissolved in a mixture of benzene derivative diluted in carbon tetrachloride ($CCl_4$) resulting in two peaks in the IR spectra (free and complexed X−H species).

**FTIR Spectroscopy.** All spectra were recorded on a Bruker Vertex 70 FTIR spectrometer equipped with a liquid nitrogen-cooled indium antimonide detector at a spectral resolution of 1 $cm^{-1}$. Samples were filled in a gas tight liquid IR cell with sapphire windows (volume ∼20 $\mu$L). Two spacers of different thickness were used to minimize interference fringes (75 and 100 $\mu$m). The spectra were baseline corrected with a spline function integrated in the Opus 5.5 software (Bruker Photonics, Billerica, MA). The diluted samples contained 20 mM indole (or 200 mM thiophenol) in hexamethylbenzene/$CCl_4$ (1:16 wt %), pentamethylbenzene/$CCl_4$ (1:9 wt %), 1,2,4,5-tetramethylbenzene/$CCl_4$ (1:8 wt %), 1,2,4-trimethylbenzene/$CCl_4$ (1:7 wt %), mesitylene/$CCl_4$ (1:7 wt %), *p*-xylene/$CCl_4$ (1:7 wt %), toluene/$CCl_4$ (1:5 wt %), benzene/$CCl_4$ (1:5 wt %), *m*-fluorotoluene (1:1 vol%), chlorobenzene/$CCl_4$ (2:3 vol%), *o*-dichlorobenzene/$CCl_4$ (1:2 vol%), and *m*-dichlorobenzene/$CCl_4$ (1:2 vol%).

Control experiments demonstrated a very similar pattern of X−H probe frequencies in the pure aromatic solvents, further supporting the notion that the fields in the specific $\pi$-hydrogen bonds are much larger than any fields due to solvation (Figure S1).

Deuteration of pyrrole was carried out by dissolving it in an excess of deuterated methanol ($CD_3OD$) and removing the solvent under vacuum. This procedure resulted in a mixture of protonated and deuterated N−D and allowed us to study the peak shifts of both N−H and N−D modes in the same samples.

An independent measure of the vibrational Stark effect and complex-induced spectral shifts on the O−H of phenol with isotopic substitution provided an excellent check for the approach in the case of O−H···$\pi$ (O−D···$\pi$) interactions.[16] Upon deuteration, the bands corresponding to N−D···$\pi$ complexes with indole are obscured by a Fermi resonance (the ratio of the peaks is concentration independent).[21] However, we were able to measure both N−H and N−D stretch modes of pyrrole in all solvents and obtained very similar shifts as for indole (see Table S3, Figure S2). Unfortunately, the N−H and N−D bands of pyrrole could not be resolved at low temperatures, and we were not able to record vibrational Stark spectra for these samples. Measuring the deuterated S−D···$\pi$ complexes with thiophenol was not possible because S−D is a very weak oscillator and its IR bands were obscured by other bands in this cluttered region of the IR spectrum.


dx.doi.org/10.1021/ja305575t | J. Am. Chem. Soc. 2012, 134, 18986−18997

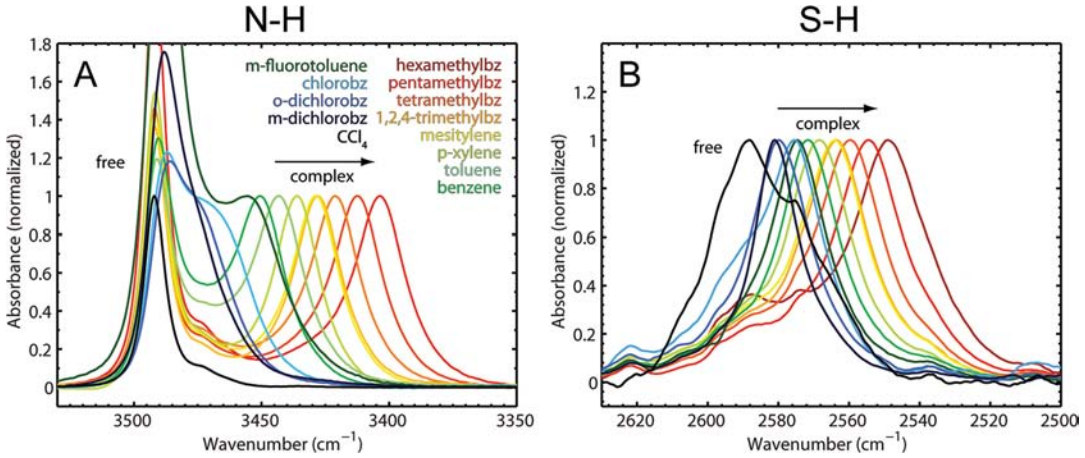


**Figure 2.** Experimental FTIR spectra. (A) N−H (indole) stretch modes in different organic solvents/$CCl_4$ mixtures. (B) S−H (thiophenol) stretch modes in different organic solvents/$CCl_4$ mixtures (bz = benzene).

**Vibrational Stark Spectroscopy.** Vibrational Stark experiments were performed at liquid nitrogen temperature in a home-built cryostat.[22] The samples were loaded into a home-built liquid cell with two sapphire windows (thickness 1 mm, diameter 13 mm, Meller Optics, Providence, RI). The windows were coated with a 45 Å layer of nickel on the surfaces facing the sample to function as a capacitor and to provide a homogeneous electric field across the sample. The windows were separated by two Teflon spacers of 26 $\mu$m thickness. Samples were frozen rapidly in liquid nitrogen into organic glasses in toluene, 2-methyl-THF, butyronitrile, *m*-fluorotoluene or a mixture of dichloromethane/dichloroethane (1:3 vol%). The concentrations varied between 0.1 and 1 M, and we tested if any concentration-dependent changes of the peaks occurred. A high-power voltage supply was connected to the cell (Trek Instruments Inc., Medina, NY), and the output voltage was synchronized with the FTIR scanning time. Spectra were acquired in rapid scan mode, and the resulting Stark spectra were the difference between 512 spectra recorded in the presence of an applied field minus 512 spectra recorded under identical conditions without field.[17] As a control, spectra were recorded at multiple electric field strengths to confirm that the Stark signals scale quadratically with the field strength, as expected for an isotropic, immobilized sample.[23] To obtain the Stark tuning rates $|\Delta\vec{\mu}_{X-H}|$ (or $|\Delta\vec{\mu}_{X-H}|\cdot f$, where $f$ is the local field correction factor),[24] the spectra were fitted using the in-house written program SpectFit.[23,25] The reported Stark tuning rates were averaged from multiple independent measurements of each sample, and the errors are given as the standard deviation. In most cases, the linear response is the primary interaction between electric field and vibrational probe, and the spectrum has a second-derivative shape.[20] In some cases the quadratic Stark effect, which is described by the difference polarizability $\Delta\bar{\alpha}_{X-H}$, can be observed as well and the resulting Stark spectrum has a first derivative shape.[17]

For the diatomic N−H and S−H probes, both stretch modes are well-defined local modes, meaning the orientation of the difference dipole $\Delta\vec{\mu}_{X-H}$ must be parallel to the bond axis.[26,27]

**DFT Calculations.** Quantum chemical calculations were performed with Gaussian 09.[28] Geometries for indole/aromatic and thiophenol/aromatic complexes were optimized using the B3LYP functional and 6-31+G(d,p) basis set.[29,30] After geometry optimization the hydrogen donor was removed, and the molecular electrostatic potential (MEP) arising only from the aromatic solvent partner in the complex was calculated.[31] The potential $\phi$ at positions X and H of the X−H bond in the X−H···$\pi$ complexes was extracted from the MEP calculations, and the projection of the electric field onto the bond is then given as the gradient of the electrostatic potential along the bond axis with the direction from X → H ($\vec{F}_{complex} = -\nabla\phi = -(\phi_X - \phi_H)/|\vec{r}_X - \vec{r}_H|$, where $\phi$ is the electrostatic potential and $\vec{r}$ the position of the atom). Binding energies were calculated for all complexes using the counterpoise (CP) method, which corrects for the basis set superposition error (BSSE).[32] For comparison, we also repeated our earlier measurements and calculations on phenol using the identical set of aromatic partners (Figure 3A).

**Fitting Procedure Employed for the Frequency Field Plots.** Since the data showed some degree of curvature, two different fitting procedures were employed. At low electric field values the plots are linear and were fitted with a linear function to extract the apparent Stark tuning rate of the free X−H species from the slope. In a second analysis intended to account for the change of $|\Delta\vec{\mu}_{X-H}|$ with field the data was fit with the sum of a quadratic and linear function, where the linear function accounts for $|\Delta\vec{\mu}_{X-H}|$ in the absence of polarization and the quadratic part for the effect of field on $|\Delta\vec{\mu}_{X-H}|$. The apparent linear Stark tuning rates in different solvents were then extracted from the gradient at the points of interest, specifically in *m*-fluorotoluene and toluene, where we can compare them to our experimental measurements of $|\Delta\vec{\mu}_{X-H}|$.

## RESULTS AND DISCUSSION

**FTIR Spectroscopy.** We used indole and thiophenol complexed with a series of aromatic compounds to study X−H···$\pi$ interactions of differing strengths. The aromatic compounds, which provide the $\pi$-hydrogen-bond acceptor, were benzene derivatives substituted with chlorine as electron-withdrawing or methyl as electron-donating groups; the substituents serve to vary the charge density of the $\pi$-system and hence the strength of the $\pi$-hydrogen bond. Because the aromatic compounds with the highest charge densities (tetra-, penta- and hexamethylbenzene) are solids, we dissolved or diluted each aromatic hydrogen-bond acceptor in carbon tetrachloride ($CCl_4$) prior to adding indole or thiophenol. We measured the vibrational frequencies of the X−H hydrogen donors in each sample and compared them to the frequencies observed in pure $CCl_4$, in which no hydrogen bonds are present.

In earlier work on O−H···$\pi$ hydrogen bonds we demonstrated that, under the conditions of these experiments, the contribution of the solvent reaction field to the observed peak shifts is negligible compared to the shifts due to complex formation.[16] The same conclusion is directly supported for our current work by the observation that the peak positions for the free X−H species are almost identical in pure $CCl_4$ and in the $CCl_4$/aromatic mixtures used to study the complexes (Figure S1). The observed peak shifts of the X−H stretch, with respect to the frequency in $CCl_4$ in which no X−H···$\pi$ interaction


dx.doi.org/10.1021/ja305575t | J. Am. Chem. Soc. 2012, 134, 18986−18997

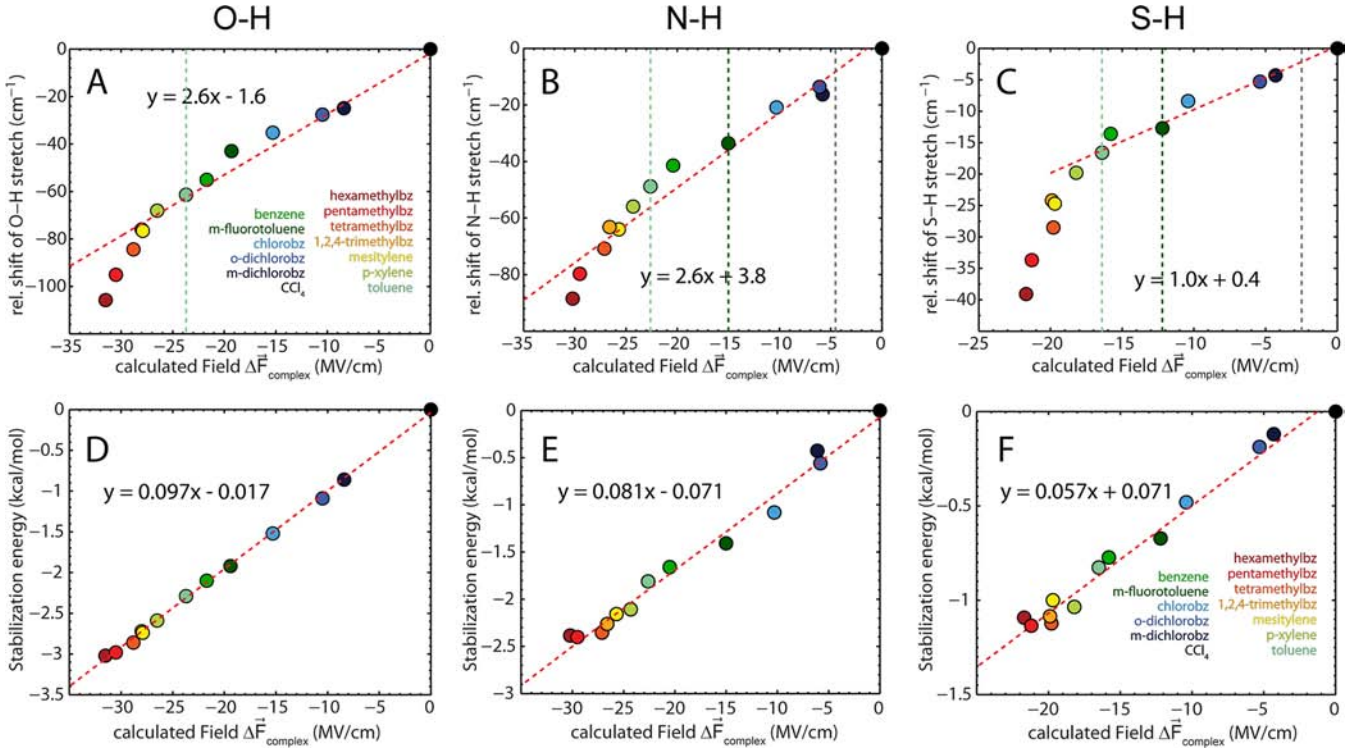


**Figure 3.** Correlation between measured X−H stretch frequencies in different hydrogen-bond complexes (diluted in $CCl_4$) and calculated electric fields arising from the aromatic hydrogen-bond acceptor based on DFT. The relative IR shift is the difference between the frequency of X−H in the aromatic/$CCl_4$ mixture and the free species in pure $CCl_4$. The dashed vertical lines represent reference points calibrated with vibrational Stark spectroscopy (X−H in toluene, *m*-fluorotoluene, and free species in DCM/DCE, see Table 2). The ground-state dipole moment of the N−H bond is larger, as compared to the S−H bond, resulting in a larger solvent reaction field for the free X−H species in DCM/DCE (Figure S3). (A) O−H···$\pi$ interaction with phenol from our previous work,[16] extended to include solvents with stronger hydrogen bonds. (B) N−H···$\pi$ interaction with indole. (C) S−H···$\pi$ interaction with thiophenol. (D−F) Correlation between calculated binding energies and electric fields both calculated with DFT. (D) O−H···$\pi$ interaction with phenol. (E) N−H···$\pi$ interaction with indole. (F) S−H···$\pi$ interaction with thiophenol.

occurs, therefore report on complex formation between the hydrogen-bond donors and the $\pi$-system of the acceptor.[33] To the extent that these shifts are electrostatic in origin, they can be converted into electric fields based on the measured vibrational Stark effect (see below), as we reported previously for phenol.[16]

**Indole.** Figure 2A shows the normalized FTIR spectra of 20 mM indole (N−H) dissolved in mixtures of $CCl_4$ and different aromatic hydrogen-bond acceptors. The IR spectra of these samples all display two peaks for the N−H vibration, corresponding to the free and complexed (N−H···$\pi$) species. The proportions of the aromatic hydrogen-bond acceptors and $CCl_4$ were adjusted for each sample to ensure roughly equal populations of free and complexed N−H (see Materials and Methods section for the concentrations used in each case). One peak is observed for the N−H stretch of indole dissolved in pure $CCl_4$, which corresponds to the free indole species (3491.5 $cm^{-1}$). The peaks corresponding to the N−H···$\pi$ complexes are all red-shifted with respect to the free species and follow a clear trend according to the electron-withdrawing or electron-donating character of the $\pi$-system (Table S1). The most red-shifted complex is formed between indole and hexamethylbenzene, which has the most electron-rich $\pi$-system (3402.6 $cm^{-1}$). The overall range of peak shifts covers ~88 $cm^{-1}$, suggesting that the sensitivity of the N−H group to electric field is similar to that of O−H (the range for O−H of phenol for the same series of $\pi$ acceptors covers ~106 $cm^{-1}$, Table S2).

**Thiophenol.** The FTIR spectra of 200 mM thiophenol (S−H) in the same solvent mixtures used for indole are shown in Figure 2B. In contrast to indole, the free thiophenol species is not observed in the solvent mixtures containing aromatic hydrogen-bond acceptors, and only single S−H bands are observed in each sample. The most blue-shifted species is free thiophenol in pure $CCl_4$ (2589 $cm^{-1}$). The peaks for the S−H stretch in all other samples are shifted to the red in the identical order as seen for the N−H and O−H stretches of indole and phenol[16] but are spread over a range of only 40 $cm^{-1}$, suggesting a smaller sensitivity to electric field for S−H. The intensities of the IR bands increase dramatically with the red-shift (Figure S4), which is not seen with indole, indicating that the transition moment (S−H 0→1) changes significantly in different thiophenol/aromatic complexes (see below).

## ■ COMPARISON WITH CALCULATED ELECTRIC FIELDS AND BINDING ENERGIES

We previously demonstrated that DFT calculations on different phenol/aromatic complexes in the gas phase accurately capture the electrostatics of the O−H···$\pi$ interaction.[16] In order to obtain a quantitative description of the electric fields involved in the other X−H···$\pi$ interactions we performed DFT calculations on the different complexes in the gas-phase. After geometry optimization of the complexes, the projection of the electric field along the X−H bond due to the aromatic complex partner (i.e., the hydrogen-bond acceptor) was calculated for

each complex (see Materials and Methods section for details of the procedure).

In order to have a reference point for the electric field at the X−H bond in the absence of a hydrogen bond we used $CCl_4$ as a reference solvent. The observed peak shifts $\Delta\tilde{\nu}^{obs}_{X-H}$, observed between $CCl_4$ and the $CCl_4$/aromatic partner mixtures, are attributed to the changes in electric field upon hydrogen bonding, given by $\Delta\vec{F}_{complex} = \vec{F}_{complex} - \vec{F}_{CCl_4}$, where $\vec{F}_{complex}$ and $\vec{F}_{CCl_4}$ represent the absolute electric fields in the hydrogen-bond complex and in $CCl_4$. We extended our earlier work on phenol to encompass the identical set of solvents used for indole and thiophenol, to facilitate a direct comparison between the O−H, N−H, and S−H···$\pi$ interactions. Plotting the measured X−H stretch frequencies against the calculated electric fields $\Delta\vec{F}_{complex}$ results in a clear correlation for O−H and N−H (Figure 3A,B), although the data display some deviation from a linear relationship at higher electric fields (see below). The calculated changes in electric field due to complex formation are as large as −30 MV/cm for the strongest interactions (between indole or phenol and hexamethylbenzene). The slope of the best fit line for N−H is 2.6 $cm^{-1}$/(MV/cm), that is a change of 1 MV/cm in electric field causes an IR peak shift of $\Delta\tilde{\nu}^{obs}_{X-H}$ = 2.6 $cm^{-1}$, very close to the observed linear Stark tuning rate in toluene (see below). The intercept of the best-fit line is close to the frequency of the free species in $CCl_4$ (+3.8 $cm^{-1}$), suggesting that the IR shifts observed on complex formation are mostly due to electrostatics. This result is very similar to our observations on O−H···$\pi$ interactions between phenol and benzene derivatives here and in previous work.[16]

For the S−H···$\pi$ complexes, a plot of the observed vibrational frequencies versus calculated field shows a stronger deviation from a linear correlation than observed with O−H and N−H (Figure 3C), implying that the IR shifts are not strictly linear with the electric field created by the hydrogen-bond acceptor. This effect is more pronounced for stronger hydrogen bonds (or larger electric fields). The data at low $\Delta\vec{F}_{complex}$ values are roughly linear, and the slope in this region is ∼1.0 $cm^{-1}$/(MV/cm), which is very similar to the measured linear Stark tuning rate of free thiophenol in the glass-forming solvent DCM/DCE (see below). The peak positions for the weaker complexes approach the peak position for the free species in $CCl_4$, again suggesting that the shifts are mostly electrostatic in origin.

To quantify the electrostatic contribution to binding, we calculated binding energies of all complexes with DFT in the gas phase. The energies range from 0 to −3 kcal/mol for the phenol/aromatic complexes, from 0 to −2.4 kcal/mol for the indole/aromatic complexes, and from 0 to −1.1 kcal/mol for thiophenol/aromatic complexes. Plotting the calculated binding energies against the calculated electric fields results in excellent linear correlations for all of the X−H···$\pi$ complexes, and the $y$-intercept occurs at zero field, i.e., the field in the absence of an interaction, indicating that the electric field experienced by the hydrogen-bond donor increases in a linear fashion with the binding energy (Figure 3D−F). The dominant part of the electrostatic interaction is likely to be the interaction of the $\pi$-system of the aromatic solvent with the dipole moment of the X−H group (the X−H group is pointing directly toward the $\pi$-system of the acceptor, and contributions from the C−H groups are small because of their small dipole moments and because they are further away from the acceptor than the X−H group). The electrostatic energy of a dipole $\vec{\mu}$ in an electric field $\vec{F}$ is given by $E = -\vec{\mu}\cdot\vec{F}$, i.e., the slopes of the linear fits in Figure 3D−F should give the apparent dipole moments $\vec{\mu}_{O-H}$, $\vec{\mu}_{N-H}$, and $\vec{\mu}_{S-H}$, and any deviations should reflect the nonelectrostatic contribution to the interaction. The slopes of the best fit lines yield apparent dipole moments $\vec{\mu}_{O-H}$ = 2.0 D, $\vec{\mu}_{N-H}$ = 1.7 D, and $\vec{\mu}_{S-H}$ = 1.2 D. Comparison with the experimental dipole moments of O−H, N−H, and S−H ($\vec{\mu}$ = 1.69 D for ethanol, $\vec{\mu}$ = 1.77 D for pyrrole, and $\vec{\mu}$ = 1.6 D for mercaptoethanol; the molecular dipole moment arises mainly from the X−H bond dipole)[34] indicates that within this level of theory, the binding energies can be considered to arise primarily from the electrostatic interaction between the X−H dipole and the field generated by the aromatic partner. Note that electron correlation is only poorly included at this level of theory (i.e., the dispersion interaction is not captured accurately). Higher level methods, like MP2 or CCSD, are necessary to include this effect properly, which could result in larger binding energies.[35−38]

## VIBRATIONAL STARK EFFECT SPECTROSCOPY AS A TOOL TO QUANTIFY ELECTRIC FIELDS EXPERIMENTALLY

The relationships observed between $\Delta\tilde{\nu}^{obs}_{X-H}$ and $\Delta\vec{F}_{complex}$ strongly suggest that the vibrational probes are responding to the electric field they experience when forming X−H···$\pi$ complexes. To obtain further evidence of this we turned to vibrational Stark effect spectroscopy. The vibrational Stark effect provides the connection between observed peak shifts and changes in the projection of electric fields along a vibrational probe's bond axis, and can be used to obtain information about its local electrostatics. If the peak shifts $\Delta\tilde{\nu}^{obs}_{X-H}$ of a hydrogen-bond donor X−H are due to the hydrogen-bonding field in the X−H···$\pi$ complexes, $\Delta\vec{F}_{complex}$, then the peak shifts are given by the purely electrostatic relationship:

$$hc\Delta\tilde{\nu}^{obs}_{X-H} = -\Delta\vec{\mu}_{X-H}\cdot\Delta\vec{F}_{complex} - \frac{1}{2}\Delta\vec{F}_{complex}\cdot\Delta\bar{\alpha}_{X-H}\cdot\Delta\vec{F}_{complex} \quad (1)$$

where $h$ is Planck's constant and $c$ the speed of light. The first term is linear with electric field and contains the parameter $|\Delta\vec{\mu}_{X-H}|$, which is called the linear Stark tuning rate. The second term is quadratic in field and contains the parameter $\Delta\bar{\alpha}$, which is called the difference polarizability. These terms arise from changes of the dipole moment and polarizability of the vibrational probe between the ground and excited states. In principle, both Stark parameters can be determined from vibrational Stark spectroscopy measurements in an external applied electric field, although for most vibrational transitions the linear component $|\Delta\vec{\mu}_{X-H}|$ dominates the response to field. The linear Stark tuning rate can therefore be used to convert frequency shifts observed in FTIR spectra, $\Delta\tilde{\nu}^{obs}_{X-H}$, into changes of the projection of electric fields along the X−H bond axis, $\Delta\vec{F}_{complex}$, according to eq 1. Note that effects other than electrostatics, such as charge transfer, can affect the IR frequency and are not described by eq 1.

In order to calibrate the sensitivity of each vibrational probe to electric field, we performed vibrational Stark experiments, in

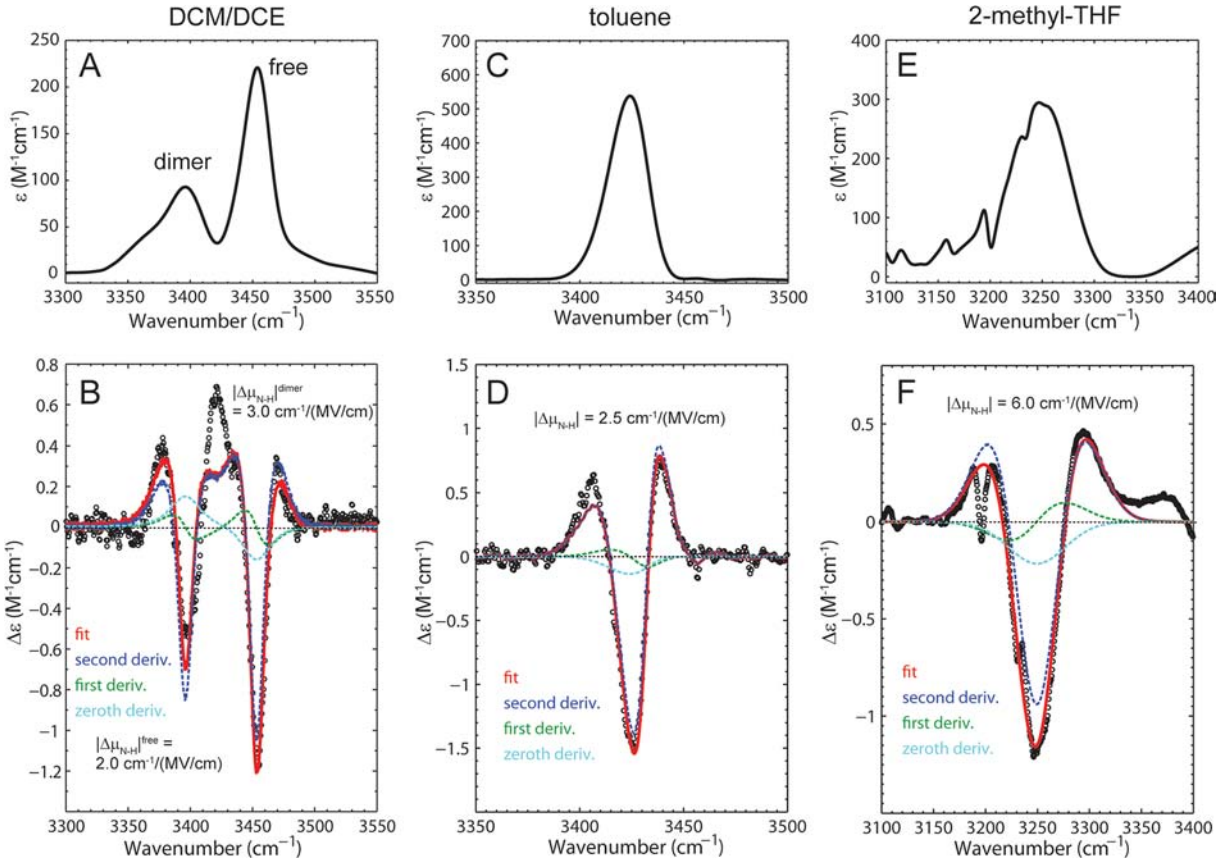


**Figure 4.** IR extinction and vibrational Stark spectra of indole in different glass-forming solvents recorded at $T$ = 77 K. (A) Extinction spectrum showing the N−H stretch in DCM/DCE ($\tilde{\nu}_{free}$ = 3450 cm$^{-1}$, $\varepsilon_{max}$ = 221 M$^{-1}$ cm$^{-1}$, and $\tilde{\nu}_{dimer}$ = 3396 cm$^{-1}$, $\varepsilon_{max}$ = 93 M$^{-1}$ cm$^{-1}$). (B) Stark spectrum scaled to an applied field of 1 MV/cm (dots) with fit (red). (C) Extinction spectrum showing the N−H stretch in toluene ($\tilde{\nu}$ = 3424 cm$^{-1}$, $\varepsilon_{max}$ = 540 M$^{-1}$ cm$^{-1}$). (D) Stark spectrum scaled to an applied field of 1 MV/cm (dots) with fit (red). (E) Extinction spectrum showing the N−H stretch in 2-methyl-THF ($\tilde{\nu}$ = 3249 cm$^{-1}$, $\varepsilon_{max}$ = 290 M$^{-1}$ cm$^{-1}$). (F) Stark spectrum scaled to an applied field of 1 MV/cm (dots) with fit (red). The small sharp features arise from absorption and Stark effects of the solvent.

which a unidirectional electric field was applied across the sample in a frozen glass solvent, and the effect on the IR spectrum was determined.[17,24] Under these conditions the response of the vibrational probe to electric field is given by eq 1, suitably averaged over all orientations. Note that the maximum applied fields that can be generated in the laboratory (<1 MV/cm) are much smaller than the microscopic fields due to complex formation.

**Free X−H Probe.** Figure 4 shows the absorbance and vibrational Stark effect spectra of indole (at 100 mM concentration) dissolved in the glass-forming solvent DCM/DCE at liquid nitrogen temperature. Note that higher concentrations of the probe molecule than were used in the FTIR experiments are necessary because of the inherently lower signal in the Stark experiments (for the highest applied electric fields, the observed changes in the absorbance are typically $10^3$ times smaller than the absorbance itself, see Figures 4 and 5). Two peaks are observed in these spectra, one corresponding to the free species (~3450 cm$^{-1}$) and the other peak most likely corresponding to a dimeric species, the indole:indole $\pi$-hydrogen bond (~3400 cm$^{-1}$).[39−41] This assignment is supported by control experiments demonstrating that the intensity of the peak at 3400 cm$^{-1}$ is strongly concentration dependent but that the peak position does not shift with concentration (Figure S5). DFT calculations suggest that a $\pi$-hydrogen-bond complex between the N−H group of one indole molecule and the six-membered ring of another is the minimum-energy structure of the dimer complex.[41]

The Stark parameters of a vibrational probe can be extracted by fitting the vibrational Stark spectrum with a linear combination of the derivatives of the absorption spectrum.[17] The magnitude of the linear Stark tuning rate is related to the second-derivative component of the fit, while the difference polarizability $\Delta\bar{\alpha}$ is related to the zeroth-, first-, and second-derivative components. The vibrational Stark effect spectrum of indole in DCM/DCE exhibits mainly second-derivative character, indicating that the Stark effects for both free and dimerized indole are dominated by the difference dipole $|\Delta\vec{\mu}_{N-H}|$. The values of the linear Stark tuning rates are $|\Delta\vec{\mu}_{N-H}|^{free}_{DCM/DCE}$ = 2.0 cm$^{-1}$/(MV/cm) for the free species and $|\Delta\vec{\mu}_{N-H}|^{dimer}_{DCM/DCE}$ = 3.0 cm$^{-1}$/(MV/cm) for the dimeric species (Table 1). These values are extracted from fits in which the peaks for the free and dimeric species were modeled as separate Gaussian functions. As an additional confirmation of these values, we performed the fitting procedure using the experimental absorption spectrum (Figure S6). The measured values of the linear Stark tuning rate correspond to the frequency shifts produced by an electric field of 1 MV/cm aligned along the N−H bond axis.

The vibrational Stark effect spectra of thiophenol were also measured in DCM/DCE but at higher concentration (600 mM) because of the weaker oscillator strength of the S−H


dx.doi.org/10.1021/ja305575t | J. Am. Chem. Soc. 2012, 134, 18986−18997

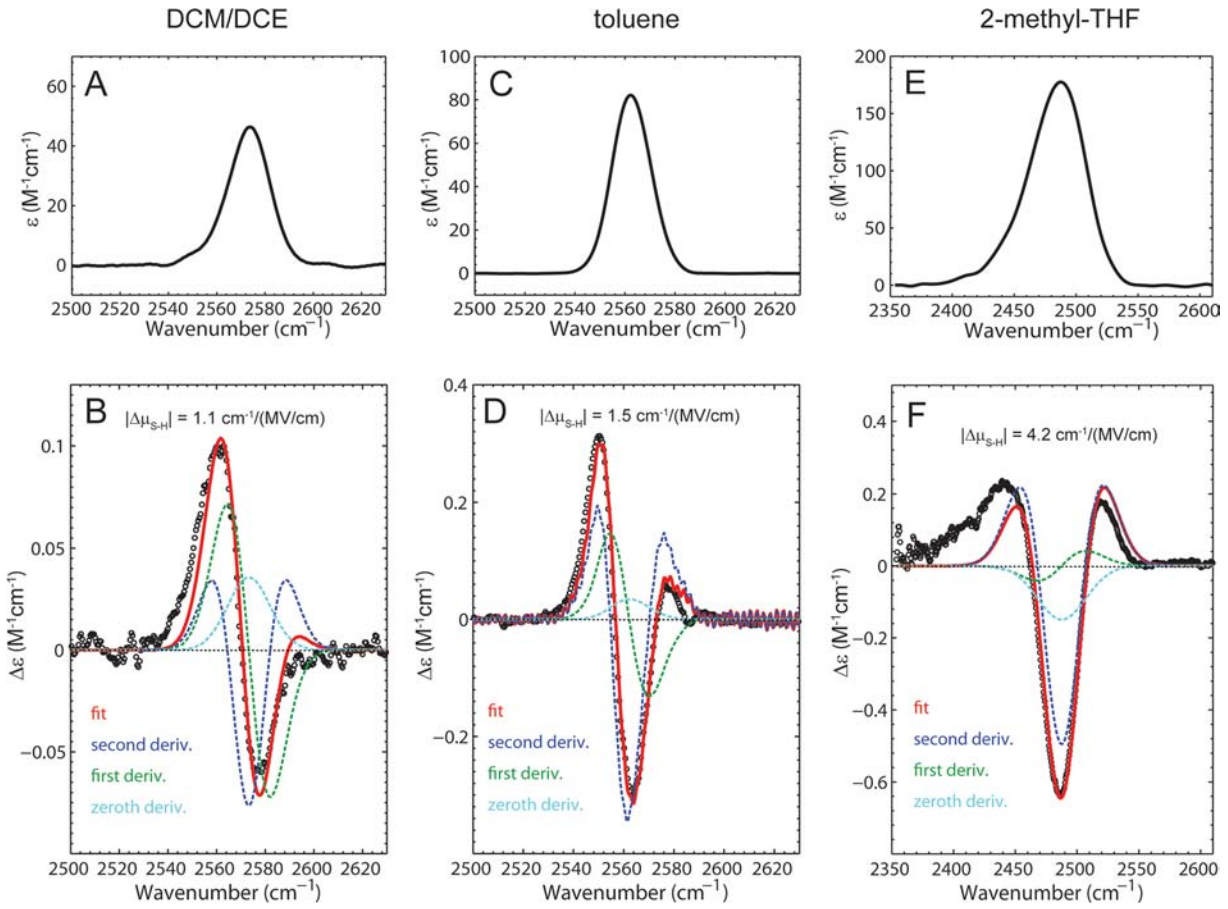


**Figure 5.** IR extinction and vibrational Stark spectra of thiophenol in different glass-forming solvents recorded at $T$ = 77 K. (A) Extinction spectrum showing the S−H stretch in DCM/DCE ($\tilde{\nu}$ = 2574 cm$^{-1}$, $\varepsilon_{max}$ = 46 M$^{-1}$ cm$^{-1}$). (B) Stark spectrum scaled to an applied field of 1 MV/cm (dots) with fit (red). (C) Extinction spectrum showing the S−H stretch in toluene ($\tilde{\nu}$ = 2562 cm$^{-1}$, $\varepsilon_{max}$ = 82 M$^{-1}$ cm$^{-1}$). (D) Stark spectrum scaled to an applied field of 1 MV/cm (dots) with fit (red). (E) Extinction spectrum showing the S−H stretch in 2-methyl-THF ($\tilde{\nu}$ = 2488 cm$^{-1}$, $\varepsilon_{max}$ = 177 M$^{-1}$ cm$^{-1}$). (F) Stark spectrum scaled to an applied field of 1 MV/cm (dots) with fit (red).

**Table 1. BSSE-Corrected Stabilization Energies of the Phenol/, Indole/, and Thiophenol/Aromatic Complexes Calculated with DFT[a]**

| | phenol | indole | thiophenol |
|---|---|---|---|
| solvent | stabilization energy (kcal/mol) | stabilization energy (kcal/mol) | stabilization energy (kcal/mol) |
| carbon tetrachloride | 0 | 0 | 0 |
| *m*-dichlorobenzene | −0.86 (0.60) | −0.43 (0.48) | −0.12 (0.55) |
| *o*-dichlorobenzene | −1.09 (0.61) | −0.56 (0.51) | −0.19 (0.59) |
| chlorobenzene | −1.52 (0.59) | −1.08 (0.51) | −0.48 (0.56) |
| *m*-fluorotoluene | −1.92 (0.69) | −1.41 (0.52) | −0.67 (0.62) |
| benzene | −2.10 (0.55) | −1.66 (0.43) | −0.77 (0.48) |
| toluene | −2.29 (0.60) | −1.81 (0.45) | −0.83 (0.56) |
| *p*-xylene | −2.59 (0.71) | −2.11 (0.54) | −1.04 (0.66) |
| mesitylene | −2.74 (0.77) | −2.16 (0.55) | −1.00 (0.74) |
| 1,2,4-trimethylbenzene | −2.72 (0.74) | −2.26 (0.57) | −1.08 (0.72) |
| 1,2,4,5-tetramethylbenzene | −2.86 (0.83) | −2.36 (0.61) | −1.12 (0.78) |
| pentamethylbenzene | −2.98 (0.86) | −2.40 (0.63) | −1.14 (0.81) |
| hexamethylbenzene | −3.02 (0.92) | −2.39 (0.67) | −1.09 (0.86) |

[a]Values in parentheses show the BSSE.

group (Figure 5). Only a single species corresponding to free thiophenol is observed in these spectra. In contrast to what we observed with indole and phenol, the vibrational Stark spectrum of the S−H stretch of thiophenol shows a significant contribution from the first derivative of the absorption, indicating that the difference polarizability $\Delta\bar{\alpha}_{S-H}$ is significant. The linear Stark tuning rate, extracted from the second-derivative contribution, is much smaller than for N−H and O−H, with a value of $|\Delta\vec{\mu}_{S-H}|_{DCM/DCE}$ = 1.1 cm$^{-1}$/(MV/cm).

The measured values of the linear Stark tuning rates of N−H and S−H probes shed further light on the correlations between the frequency shifts of the X−H probes and the calculated field


dx.doi.org/10.1021/ja305575t | J. Am. Chem. Soc. 2012, 134, 18986−18997

in each X−H···$\pi$ complex (Figure 3). The linear Stark tuning rates agree reasonably well with the slopes of these correlations, particularly if one focuses on the region of the plots where the fields are small, corresponding to the weaker complexes. The smaller linear Stark tuning rate of the S−H probe explains why the observed shifts for the S−H···$\pi$ complexes are consistently smaller than those of the other probes. These observations are strong evidence that the vibrational Stark effect is the primary mechanism underlying the frequency shifts observed in the different X−H···$\pi$ complexes. However, in the region of the plots corresponding to the stronger X−H···$\pi$ complexes, the apparent slopes are considerably larger than the measured linear Stark tuning rates. This discrepancy led us to wonder whether the linear Stark tuning rates increase when the probes are engaged in stronger complexes.

## BOND POLARIZATION ENHANCES VIBRATIONAL STARK EFFECTS IN HYDROGEN BONDS

To understand why the measured vibrational frequency shifts and calculated electric fields display deviations from a linear correlation, we investigated the influence of different environments on the vibrational Stark spectra of the different hydrogen-bond donors. We recorded vibrational Stark spectra of the hydrogen-bond donors indole and thiophenol in different glass-forming solvents at 77 K (many of the solvents used as hydrogen-bond acceptors do not form optical quality glasses at 77K and could not be used for this analysis). We used toluene and *m*-fluorotoluene, which form weak X−H···$\pi$ hydrogen bonds, and 2-methyl-THF and butyronitrile, which form moderate hydrogen bonds of the X−H···O and X−H···N type, respectively.

**Weak X−H···$\pi$ Hydrogen-Bond Regime.** The vibrational Stark effect spectrum of 200 mM indole in toluene is shown in Figure 4D and contains only one peak, which corresponds to the hydrogen-bonded complex between the N−H of indole and the $\pi$-face of toluene. The spectrum is dominated by second-derivative character, and the Stark tuning rate is $|\Delta\vec{\mu}_{N-H}|_{toluene}$ = 2.5 cm$^{-1}$/(MV/cm), a value that is significantly larger than that of the free species measured above.

The vibrational Stark effect spectrum of 200 mM indole in *m*-fluorotoluene shows three peaks, which we assign to the free species: the dimeric form (the peak position is close to that of the dimeric form in DCM/DCE) and the complex with *m*-fluorotoluene (Figure S7). The Stark tuning rates for free and dimeric species are $|\Delta\vec{\mu}_{N-H}|^{free}_{m\text{-fluorotolune}}$ = 2.0 cm$^{-1}$/(MV/cm) and $|\Delta\vec{\mu}_{N-H}|^{dimer}_{m\text{-fluorotolune}}$ = 3.0 cm$^{-1}$/(MV/cm), in perfect agreement with the data obtained in DCM/DCE, while the third peak has a sensitivity of $|\Delta\vec{\mu}_{N-H}|_{m\text{-fluorotolune}}$ = 2.3 cm$^{-1}$/(MV/cm).

The vibrational Stark effect spectrum of 600 mM thiophenol obtained in toluene is shown in Figure 5D. The spectrum displays a greater degree of second-derivative character than observed in DCM/DCE, and the linear Stark tuning rate is larger than that of the free species, with $|\Delta\vec{\mu}_{S-H}|_{toluene}$ = 1.5 cm$^{-1}$/(MV/cm). The vibrational Stark effect spectrum in *m*-fluorotoluene shows an intermediate degree of first and second derivative character, and the linear Stark tuning rate is $|\Delta\vec{\mu}_{S-H}|_{m\text{-fluorotolune}}$ = 1.3 cm$^{-1}$/(MV/cm) (Figure S8).

These results for the N−H and S−H stretches reveal for the first time that the linear Stark tuning rate, rather than being an intrinsic property of the chemical bond, can change significantly due to the formation of chemical interactions. We are now in a position to explain the deviations from linearity observed in Figure 3. In our earlier work on phenol, the observed vibrational frequency of the O−H group was found to correlate in a linear fashion with the calculated field for the O−H···$\pi$ complexes. However, in that earlier work we did not include the stronger hydrogen-bond acceptors tetramethylbenzene, pentamethylbenzene, and hexamethylbenzene used in the current study. With the inclusion of these complexes it becomes apparent that the O−H frequency shifts do deviate somewhat from a linear correlation at high fields (Figure 3A). A similar degree of curvature is present in the data for the N−H stretch (Figure 3B), while for the S−H stretch, shown in Figure 3C, the curvature is much more pronounced. These observations can be accounted for by our vibrational Stark effect measurements, which show for a given X−H probe that the formation of progressively stronger X−H···$\pi$ complexes results in progressively larger linear Stark tuning rates and that these effects are most dramatic for the S−H probe. The X−H···$\pi$ complexes for which the values of the linear Stark tuning rates were experimentally determined (*m*-fluorotoluene and toluene) are highlighted in Figure 3 by vertical dotted lines. The slope of the curves at these points can be considered to represent apparent linear Stark tuning rates, and these values were estimated by fitting the data to the sum of a linear and a quadratic term (see Materials and Methods section for the procedure used). For the N−H probe, the values of the slopes are 1.7 for the complex with *m*-fluorotoluene and 2.7 for the complex with toluene, which can be compared to the measured linear Stark tuning rates of 2.3 and 2.5 cm$^{-1}$/(MV/cm), respectively. For the S−H probe, the values of the slopes are 1.6 for *m*-fluorotoluene and 2.2 for toluene, and the measured linear Stark tuning rates are 1.3 and 1.5 cm$^{-1}$/(MV/cm). This reasonable agreement indicates that an important reason for the curvature observed in the plots of Figure 3 is that the linear Stark tuning rates increase for stronger complexes. The slopes of the curves are in all four cases larger than the measured linear Stark tuning rate, suggesting that other effects may contribute to the curvature.

The differing extent to which each probe's linear Stark tuning rate is effected by complex formation can be attributed to differences in the atomic polarizabilities of the atoms comprising the X−H probe, which increase in the order O < N ≪ S. The more polarizable the probe, the greater the increase in the linear Stark tuning rate in the stronger X−H···$\pi$ complexes, leading to small deviations from a linear correlation for O−H and N−H and strong deviations for S−H (the influence of polarizability on the linear Stark tuning rate is discussed in greater detail below).

In principle the deviations from linear correlations observed in Figure 3 could be due to a significant difference polarizability, $\Delta\bar{\alpha}_{X-H}$, rather than from increasing magnitudes of the linear Stark tuning rates $|\Delta\vec{\mu}_{X-H}|$ (see eq 1). In a previous study on nitriles the difference polarizability $\Delta\bar{\alpha}$ was determined experimentally from the zeroth-, first-, and second-derivative components of the fits to the Stark spectrum. Unfortunately our data are not of sufficient quality to allow us to determine the difference polarizability $\Delta\bar{\alpha}_{X-H}$, for which very high signal-to-noise is required in both the absorbance and Stark spectra in order to obtain accurate values for the zeroth- and first-derivative contributions to the Stark spectrum. This is because of the much greater line width of the X−H modes (the intensity of the Stark signal scales with the square root of the line width)[17] as well as the fact that we had to use lower

Table 2. Stark Parameters of the Hydrogen-Bond Donors N−H and S−H in Different Glass-Forming Solvents at $T$ = 77 K (cf. Figures 4−6)

| | N−H | | | S−H | | |
|---|---|---|---|---|---|---|
| solvent | $\lvert\Delta\vec{\mu}_{N-H}\rvert \cdot f^a$ (cm$^{-1}$/(MV/cm)) | $\lvert\vec{M}_{N-H}\rvert$ (D) | $q_{N-H}$ (e) | $\lvert\Delta\vec{\mu}_{S-H}\rvert \cdot f^a$ (cm$^{-1}$/(MV/cm)) | $\lvert\vec{M}_{S-H}\rvert$ (D) | $q_{S-H}$ (e) |
| DCM/DCE | 2.0 ± 0.3 | 0.2419 | 0.70 | 1.1 ± 0.1 | 0.1026 | 0.26 |
| *m*-fluorotoluene | 2.3 ± 0.3 | 0.2780 | 0.80 | 1.3 ± 0.1 | 0.0863 | 0.22 |
| toluene | 2.5 ± 0.1 | 0.2648 | 0.76 | 1.5 ± 0.1 | 0.1148 | 0.29 |
| butyronitrile | 6.1 ± 0.2 | 0.3084 | 0.88 | 2.6 ± 0.2 | 0.1675 | 0.42 |
| 2-methyl-THF | 6.0 ± 0.2 | 0.3956 | 1.11 | 4.2 ± 0.3 | 0.2897 | 0.72 |

[a] $f$ is the local field correction factor (for more details see Bublitz and Boxer).[24]

concentration samples to prevent dimer formation. Qualitatively we observe that across the series of solvents, in which progressively stronger interactions are formed, the contributions to the Stark spectra from the zeroth and first derivative of the absorption spectra remain similar, while the second-derivative contribution increases significantly. This indicates that the primary effect of hydrogen bonds is to increase the linear Stark tuning rate. As discussed above our data strongly suggest that the effects seen in Figure 3 can be mostly accounted for by variations in the magnitude of $\lvert\Delta\vec{\mu}_{X-H}\rvert$ caused by interactions of differing strength, but we cannot rule out a contribution from $\Delta\bar{\alpha}_{X-H}$.

**Moderate X−H···O and X−H···N Hydrogen-Bond Regime.** In 2-methyl-THF, indole forms a N−H···O hydrogen bond of moderate strength resulting in a large red shift of the N−H band (~3250 cm$^{-1}$ relative to 3450 cm$^{-1}$ for the free species in DCM/DCE). This band displays a very strong feature in the Stark spectrum, which has mainly second-derivative shape, and $\lvert\Delta\vec{\mu}_{N-H}\rvert_{2\text{-methyl-THF}}$ = 6.0 cm$^{-1}$/(MV/cm). This value represents the largest linear Stark tuning rate measured so far for any vibrational transition (Figure 4).[20] In butyronitrile indole forms a N−H···N hydrogen bond (redshift from 3491.5 to 3332 cm$^{-1}$) with a Stark tuning rate $\lvert\Delta\vec{\mu}_{N-H}\rvert_{\text{butyronitrile}}$ = 6.1 cm$^{-1}$/(MV/cm), very similar to the previous case (Figure S7).

The same phenomenon is observed for thiophenol dissolved in 2-methyl-THF (Figure 5). The IR absorbance band corresponding to the S−H stretch is shifted dramatically to the red with respect to the free species (~2490 versus 2574 cm$^{-1}$) accompanied by an increase in the extinction coefficient. In contrast to what was observed in the other glass-forming solvents, the shape of the Stark spectrum is exclusively second derivative in character, and a dramatic increase in its Stark tuning rate is observed to $\lvert\Delta\vec{\mu}_{S-H}\rvert_{2\text{-methyl-THF}}$ = 4.4 cm$^{-1}$/(MV/cm). In butyronitrile thiophenol forms an S−H···N hydrogen bond, the S−H stretch redshifts by ~28 cm$^{-1}$, and the Stark tuning rate is $\lvert\Delta\vec{\mu}_{S-H}\rvert_{\text{butyronitrile}}$ = 2.6 cm$^{-1}$/(MV/cm) (see Figure S8). Thus the effect of these stronger hydrogen bonds is to perturb the linear Stark tuning rates of the probes by an even greater amount than observed with the weaker X−H···$\pi$ complexes.

**Physical Origin of the Variation in Linear Stark Tuning Rates.** The linear Stark tuning rate $\lvert\Delta\vec{\mu}_{X-H}\rvert$ can arise from two distinct physical effects, the anharmonicity of the bond $\lvert\Delta\vec{\mu}^{anh}_{X-H}\rvert$ and the field dependence of the force constant of the bond $\lvert\Delta\vec{\mu}^{bond}_{X-H}\rvert$ due to electronic polarizability.[19,23] It is possible to quantify these individual contributions because the Stark tuning rate obtained by vibrational Stark effect spectroscopy is the sum of both effects, and the contribution of anharmonicity can be calculated using quantum mechanical models.[19,23] To shed light on the origin of the large values of $\lvert\Delta\vec{\mu}_{X-H}\rvert$ for the hydrogen-bond donors used in this study as well as why these values vary in different chemical interactions, we assessed the contribution of anharmonicity $\lvert\Delta\vec{\mu}^{anh}_{X-H}\rvert$ to the linear Stark tuning rates.

The anharmonic contribution to the linear Stark tuning rate can be interpreted as a displacement of the effective charge of the oscillator, $q$, by a distance $\Delta x$ (the displacement is due to the anharmonic character of the bond) and is given by

$$\lvert\Delta\vec{\mu}^{anh}_{X-H}\rvert = q\cdot\Delta x \tag{2}$$

When the X−H bond engages in chemical interactions of different strengths, the resulting electric fields will polarize the bond to different degrees, with the result that the effective charge $q$ changes somewhat in each interaction.

In a previous study on vibrtional Stark effects of several nitriles, it was shown that the linear Stark tuning rate of a vibrational transition (also referred to as the difference dipole) correlates linearly with the magnitude of the transition moment.[17] The existence of a correlation can be understood by considering the expression for the transition moment of a harmonic oscillator $\lvert\vec{M}_{X-H}\rvert$,

$$\lvert\vec{M}_{X-H}\rvert = \frac{q}{2\pi}\sqrt{\frac{h}{2mc\tilde{\nu}}} \tag{3}$$

where $q$ is the effective charge of the oscillator and $m$ its reduced mass.[17,42] Because both $\lvert\vec{M}_{X-H}\rvert$ and $\lvert\Delta\vec{\mu}_{X-H}\rvert$ depend linearly on $q$, these parameters are expected to correlate linearly among a set of chemical bonds with different values of $q$ but similar anharmonicities.

The transition moments and difference dipoles that we measured for thiophenol and indole in different solvents are summarized in Table 2, and a correlation is indeed observed (Figure 6). Note that in this study the same molecule is investigated in different environments, whereas the previous study was focused on different molecules in the same environment. Using eq 3 we estimated the effective charge of the N−H and S−H probes in each chemical environment for which both linear Stark tuning rates and transition moments were measured (see Table 2). The effective charge for S−H changes nearly 3-fold across this series of environments, whereas the effective charge of N−H changes only about 1.5-fold. This can be explained by the differences in atomic polarizabilities between nitrogen and sulfur and indicates that the S−H bond gets polarized to a larger extent than the N−H bond. Plotting the Stark tuning rates versus the transition moments results in a linear relationship between $\lvert\vec{M}_{S-H}\rvert$ and $\lvert\Delta\vec{\mu}_{S-H}\rvert$ for all investigated hydrogen bonds, even though the


dx.doi.org/10.1021/ja305575t | J. Am. Chem. Soc. 2012, 134, 18986−18997

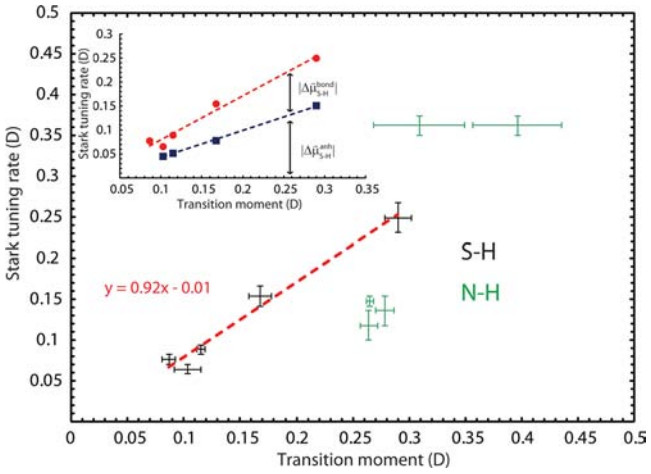


**Figure 6.** Correlation of Stark tuning rates with transition moments of S−H and N−H in different chemical environments (hydrogen bonds of differing strengths). The inset shows the contribution of anharmonicity (blue squares, calculated in the Supporting Information) to the experimentally obtained Stark tuning rate (red dots).

character of the bond is perturbed to a larger extent than the nitriles in the previous study.[17] The slope of the best fit line is 0.92 with an intercept of −0.01. This suggests that the one-dimensional oscillator model may be valid within both hydrogen-bond regimes investigated in this study. In principle, such a plot could be used to calibrate the sensitivity of the probe to electric field using experimental measurements of the transition moments, which are much less demanding than the vibrtional Stark effect experiments. For N−H the plot shows more scatter, which most likely arises from errors in the determination of transition moments due to the presence of multiple species.

To estimate the contribution of anharmonicity to the linear Stark tuning rates of the X−H probes, we calculated expectation values for the bond lengths in the vibrational ground and first excited state based on the anharmonic oscillator Morse potential for all X−H bonds (Supporting Information).[43] Here the Morse potential was parametrized using experimental values for the anharmonicity obtained from the literature. The calculated difference in bond length corresponds to the displacement $\Delta x_{X-H}$ in eq 2. Using the experimental effective charge $q$ (as derived above), we obtain from eq 2 the contribution of anharmonicity to the linear Stark tuning rate of 90% for N−H and 69% for S−H (93% for O−H from our previous work,[16] 39% for CN of acetonitrile and 47% for CN of 4-chlorobenzonitrile).[23] These values are for the free X−H species in DCM/DCE. As an additional control, we measured anharmonicities of the S−H stretch in a few representative complexes using pump−probe experiments (free S−H species, weak and moderate hydrogen bonds, see Figure S9). The anharmonicity changes slightly between the free species and the complex with toluene (100 vs 103 $cm^{-1}$), while it changes significantly between the free species and the S−H···2-methyl-THF hydrogen bond (100 vs 130 $cm^{-1}$). Calculation of the anharmonic contribution to the linear Stark tuning rate for these cases shows that the relative contribution actually stays roughly constant at ∼50−60%, even though the anharmonicity itself increases (see inset in Figure 6). This indicates that the effect of electric field on the force constant of the bond $|\Delta\vec{\mu}^{bond}_{X-H}|$, which must account for the difference, increases with the strength of S−H···X hydrogen bonds, which can be attributed to the larger polarizability of the sulfur atom compared to nitrogen and oxygen.

Taken together, this analysis nicely accounts for the variation of $|\Delta\vec{\mu}_{X-H}|$ observed in different environments. For the X−H···$\pi$ complexes the anharmonicity is constant and the increase in $|\Delta\vec{\mu}_{X-H}|$ can be attributed to an increase in the effective charge $q$ as well as an increase in the effect of the electric field on the bond's force constant, $|\Delta\vec{\mu}^{bond}_{X-H}|$, both of which are due to polarizability. For the X−H···O/N hydrogen bonds, the anharmonicity, the effective charge, and the effect of the field on the force constant all increase giving rise to very large increases in $|\Delta\vec{\mu}_{X-H}|$.

## CONCLUSION

In this paper we have measured the electrostatic component of a large number of X−H···$\pi$ hydrogen bonds. The electrostatic interaction energies derived in this manner can be compared to either experimental values of dissociation enthalpies (or similar observables) or, as we have done here, binding energies calculated using quantum chemical methods, which contain contributions from all energetically relevant interactions (electrostatics, polarization, dispersion, etc.). Such a comparison enables one to decompose the energetics of hydrogen bonds into their electrostatic and nonelectrostatic parts. By employing experiment and calculations in tandem, we have shown that it is possible to account for the response of the probe, even when the response is not strictly linear, allowing this approach to be extended to stronger hydrogen-bonding interactions. Our work thereby underscores the general utility of vibrational probes for dissecting the energetics of intermolecular interactions.

A major finding from our work is that the linear Stark tuning rate of a hydrogen-bond donor is not necessarily constant but is a function of the group's chemical environment. The degree to which hydrogen bonding perturbs the probe's response to field depends strongly on the probe's polarizability. This finding is supported by three independent observations. For probes with increasingly polarizable substituent atoms we observe: (1) progressively greater deviations from a linear correlation between observed vibrational frequency shifts and calculated electric field when the fields are large; (2) progressively larger influence of environment on the measured linear Stark tuning rate; and (3) progressively greater changes in the transition moment for the vibrational transition. While for weak hydrogen bond changes in $|\Delta\vec{\mu}_{X-H}|$ of up to 40% are observed, we find that moderate hydrogen bonds result in much more dramatic changes in probe sensitivity (up to 3-fold increases in $|\Delta\vec{\mu}_{X-H}|$). This result underscores that, for cases in which a vibrational probe is hydrogen bonded, care must be taken in interpreting observed IR shifts in terms of changes in electric field, as the vibrational probe's response to field can be heavily perturbed by the interaction.

An analogous behavior has been observed for the lowest energy electronic transition of the carotenoid spheroidene embedded in the LH2 antenna complex of *Rhodobacter sphaeroides*.[44,45] Carotenoids, such as spheroidene, are highly polarizable, and this is reflected in a large first derivative contribution to the electronic Stark line shape for free spheroidene in a frozen glass. In contrast, when bound in the LH2 complex, spheroidene experiences the electric field of the organized environment of the protein, and this induces a very

large difference dipole moment so that the Stark spectrum in the protein is completely dominated by a second-derivative line shape.

Such nonlinear behavior has not previously been observed for vibrational probes and is likely revealed in this study because of the magnitude of the fields involved, which are on the order of ±30 MV/cm for the weak X−H···$\pi$ hydrogen bonds and most likely larger for moderate hydrogen bonds. Most previous applications of vibrational probes, in contrast, involved studies of solvent fields or measurements in proteins, where calculations suggest the fields are on the order of ±10 MV/cm.[20] It is worth noting that for the weakest S−H···$\pi$ interactions studied here (e.g., the complexes with *m*-fluorotoluene, chlorobenzene, and dichlorobenzene, see Figure 3C), the fields are in this weaker regime, and the response of S−H to field appears to be roughly linear. In agreement with our results, an earlier DFT study on 4-chloro-benzonitrile demonstrated that the linear relationship between electric field and vibrational frequency is expected to break down at very large electric fields.[46]

The S−H stretch occurs in a spectral window that is free of any protein and solvent bands (~2600 $cm^{-1}$) and so could in principle be useful for studies of biomolecules. While S−H probes are difficult to detect in biological systems due to their small extinction coefficients, the increases in band intensities that result from polarization effects can nonetheless permit studies in biomolecules, and polarized cysteine S−H groups have been used to detect local dynamics in proteins.[47] Our results indicate that in such cases care must be taken in interpreting peak shifts in terms of electrostatics, as the same polarization effects that facilitate detection also alter the probe's response to field. However, we have also demonstrated that it is possible to calibrate the sensitivity of the probe in different field regimes, potentially allowing such an interpretation to be made.

## ■ ASSOCIATED CONTENT

### Supporting Information

Additional FTIR spectra, vibrational Stark spectra, control experiments, calculations of bond lengths, pump−probe experiments. Complete ref 28. This material is available free of charge via the Internet at http://pubs.acs.org.

## ■ AUTHOR INFORMATION


### Corresponding Author

miguel.saggu@gmail.com; nickl@stanford.edu; sboxer@stanford.edu


### Notes

The authors declare no competing financial interest.

## ■ ACKNOWLEDGMENTS

We thank Stephen D. Fried for his help with the anharmonic oscillator model. Chiara Giammanco in the Fayer lab performed the pump−probe experiments shown in Figure S9 and is gratefully acknowledged. M.S. was funded by a DFG Forschungsstipendium (Deutsche Forschungsgemeinschaft, SA 2156/1-1). N.M.L. was supported by a NIH Ruth L. Kirschstein National Research Service Award (F32 GM087896-03). We greatly appreciate long-standing support for this work from the NIH (GM27738) and the NSF Biophysics Program (MCB0918782).

## ■ REFERENCES


(1) Jeffrey, G. A. *An introduction to hydrogen bonding*; Oxford University Press: New York, 1997.
(2) Desiraju, G. R.; Steiner, T. *The weak hydrogen bond in structural chemistry and biology*; Oxford University Press: New York, 2001.
(3) Grabowski, S. J. *Hydrogen bonding: new insights*; Springer Verlag: New York, 2006.
(4) Morokuma, K. *Acc. Chem. Res.* **1977**, *10*, 294−300.
(5) Steiner, T. *Angew. Chem.* **2002**, *41*, 48−76.
(6) Burley, S. K.; Petsko, G. A. *Science* **1985**, *229*, 23−28.
(7) Nishio, M. *CrystEngComm* **2004**, *6*, 130−158.
(8) Brandl, M.; Weiss, M. S.; Jabs, A.; Suhnel, J.; Hilgenfeld, R. *J. Mol. Biol.* **2001**, *307*, 357−377.
(9) Steiner, T.; Koellner, G. *J. Mol. Biol.* **2001**, *305*, 535−557.
(10) Tsuzuki, S.; Honda, K.; Uchimaru, T.; Mikami, M.; Tanabe, K. *J. Am. Chem. Soc.* **2000**, *122*, 11450−11458.
(11) Biswal, H. S.; Wategaonkar, S. *J. Phys. Chem. A* **2009**, *113*, 12774−12782.
(12) Van Duijnen, P. T.; Swart, M. *J. Phys. Chem. A* **1998**, *102*, 2399−2407.
(13) Tsuzuki, S.; Fujii, A. *Phys. Chem. Chem. Phys.* **2008**, *10*, 2584−2594.
(14) Tsuzuki, S.; Honda, K.; Uchimaru, T.; Mikami, M.; Tanabe, K. *J. Am. Chem. Soc.* **2000**, *122*, 3746−3753.
(15) Zheng, J. R.; Fayer, M. D. *J. Am. Chem. Soc.* **2007**, *129*, 4328−4335.
(16) Saggu, M.; Levinson, N. M.; Boxer, S. G. *J. Am. Chem. Soc.* **2011**, *133*, 17414−17419.
(17) Andrews, S. S.; Boxer, S. G. *J. Phys. Chem. A* **2000**, *104*, 11853−11863.
(18) Boxer, S. G. *J. Phys. Chem. B* **2009**, *113*, 2972−2983.
(19) Park, E. S.; Boxer, S. G. *J. Phys. Chem. B* **2002**, *106*, 5800−5806.
(20) Suydam, I. T.; Boxer, S. G. *Biochemistry* **2003**, *42*, 12050−12055.
(21) Fritzsche, H. *Spectrochim. Acta* **1966**, *22*, 1139−1147.
(22) Andrews, S. S.; Boxer, S. G. *Rev. Sci. Instrum.* **2000**, *71*, 3567−3569.
(23) Andrews, S. S.; Boxer, S. G. *J. Phys. Chem. A* **2002**, *106*, 469−477.
(24) Bublitz, G. U.; Boxer, S. G. *Annu. Rev. Phys. Chem.* **1997**, *48*, 213−242.
(25) Andrews, S. *SpectFit*, version 2.0; Smoldyn: Seattle, WA; http://www.smoldyn.org/andrews/software.html.
(26) Li, H. M.; Wurrey, C. J.; Thomas, G. J. *J. Am. Chem. Soc.* **1992**, *114*, 7463−7469.
(27) Singh, D. K.; Srivastava, S. K.; Ojha, A. K.; Asthana, B. P. *Spectrochim. Acta A* **2008**, *71*, 823−829.
(28) Frisch, M. J. et al., *Gaussian 09*, revision A.02., Gaussian, Inc.: Wallingford, CT, 2009.
(29) Becke, A. D. *J. Chem. Phys.* **1993**, *98*, 5648−5652.
(30) Lee, C. T.; Yang, W. T.; Parr, R. G. *Phys. Rev. B* **1988**, *37*, 785−789.
(31) Johnson, B. G.; Gill, P. M. W.; Pople, J. A.; Fox, D. J. *Chem. Phys. Lett.* **1993**, *206*, 239−246.
(32) Boys, S. F.; Bernardi, F. *Mol. Phys.* **1970**, *19*, 553−566.
(33) Rosenfeld, D. E.; Gengeliczki, Z.; Fayer, M. D. *J. Phys. Chem. B* **2009**, *113*, 13300−13307.
(34) Lide, D. R. *CRC handbook of chemistry and physics*; CRC Press: Boca Raton, FL, 2005.
(35) Head-Gordon, M.; Pople, J. A.; Frisch, M. J. *Chem. Phys. Lett.* **1988**, *153*, 503−506.
(36) Møller, C.; Plesset, M. S. *Phys. Rev.* **1934**, *46*, 618−622.
(37) Pople, J. A.; Head-Gordon, M.; Raghavachari, K. *J. Chem. Phys.* **1987**, *87*, 5968−5975.
(38) Scuseria, G. E.; Schaefer, H. F., III *J. Chem. Phys.* **1989**, *90*, 3700−3703.
(39) Pejov, L. *Chem. Phys. Lett.* **2001**, *339*, 269−278.

(40) Biswal, H. S.; Gloaguen, E.; Mons, M.; Bhattacharyya, S.; Shirhatti, P. R.; Wategaonkar, S. *J. Phys. Chem. A* **2011**, *115*, 9485−9492.
(41) Geng, Y.; Takatani, T.; Hohenstein, E. G.; Sherrill, C. D. *J. Phys. Chem. A* **2010**, *114*, 3576−3582.
(42) Hush, N. S.; Reimers, J. R. *J. Phys. Chem.* **1995**, *99*, 15798−15805.
(43) Tipping, R. H.; Ogilvie, J. F. *J. Chem. Phys.* **1983**, *79*, 2537−2540.
(44) Gottfried, D. S.; Steffen, M. A.; Boxer, S. G. *Science* **1991**, *251*, 662−665.
(45) Gottfried, D. S.; Steffen, M. A.; Boxer, S. G. *Biochim. Biophys. Acta* **1991**, *1059*, 76−90.
(46) Dalosto, S. D.; Vanderkooi, J. M.; Sharp, K. A. *J. Phys. Chem. B* **2004**, *108*, 6450−6457.
(47) Kozinski, M.; Garrett-Roe, S.; Hamm, P. *J. Phys. Chem. B* **2008**, *112*, 7645−7650.